Microwave spectroscopy of a Cooper pair beam splitter

Audrey Cottet

Laboratoire Pierre Aigrain, Ecole Normale Supérieure, CNRS UMR 8551, Laboratoire associé aux universités Pierre et Marie Curie et Denis Diderot, 24, rue Lhomond, 75231 Paris Cedex 05, France

(Received 10 May 2012; revised manuscript received 23 July 2012; published 6 August 2012)

This article discusses how to demonstrate the entanglement of the split Cooper pairs produced in a double-quantum-dot based Cooper pair beam splitter (CPS), by performing the microwave spectroscopy of the CPS. More precisely, one can study the dc current response of such a CPS to two on-phase microwave gate irradiations applied to the two CPS dots. Some of the current peaks caused by the microwaves show a strongly nonmonotonic variation with the amplitude of the irradiation applied individually to one dot. This effect is directly due to a subradiance property caused by the coherence of the split pairs. Using realistic parameters, one finds that this effect has a measurable amplitude.

DOI: 10.1103/PhysRevB.86.075107 PACS number(s): 73.23.−b, 73.63.Fg, 03.67.Bg

I. INTRODUCTION

Quantum entanglement between spatially separated particles represents a promising resource in the field of quantum computation and communication. However, this fascinating behavior can be difficult to observe in practice due to decoherence caused by the particles environment. This is why the "spooky action at a distance" was first demonstrated with photons, atoms, or ions that can be naturally placed in weakly interacting conditions.[1–3]

Observing electronic entanglement in solid state systems is *a priori* more challenging since an electronic fluid is characterized by a complex many-body state in general. However, quantum entanglement has been recently observed on superconducting chips.[4] In this case, the particles are replaced by superconducting quantum bits, which can be sufficiently well isolated from the outside world thanks to the rigidity of the superconducting phase, if an appropriate circuit design is used. In these experiments, the entangled degrees of freedom are defined from the charges of small superconducting islands, or from the persistent current states of a superconducting loop, for instance.[5]

Superconductors enclose another natural source of entanglement that has not been exploited so far, i.e., the spin entanglement of its Cooper pairs. In a conventional superconductor, Cooper pairs gather two electrons correlated in a spin-singlet state. The use of this resource for entanglement production requires to build hybrid circuits in which the superconductors are connected to nonsuperconducting elements that allow the spatial separation of Cooper pairs. In principle, a double quantum dot circuit connected to a central superconducting contact (input) and two outer normal metal contacts (outputs) facilitates this process.[6] Such a "Cooper pair splitter" (CPS) has been realized recently by using double dots formed inside semiconducting nanowires[7–9,12] or carbon nanotubes.[10,11] The spatial splitting of the Cooper pairs has been demonstrated from an analysis of the current response of the CPS to a dc voltage bias. It has been theoretically suggested to use the noise cross correlations of the electrical current to reveal the entanglement of the pairs of electrons.[13–22] On the experimental side, positive cross correlations have been very recently observed between the two outputs of a CPS, an effect attributed to the existence of split Cooper pairs.[12] However, coherence was not directly measured in this experiment.

Alternatively, Ref. 23 proposes to put in evidence spin entanglement by coupling the CPS to a microwave cavity. In this reference, a double quantum dot formed inside a single wall carbon nanotube is considered. Spin-orbit interaction produces a coupling between electronic spins and cavity photons. Such a coupling leads to a lasing effect which involves a transition between the spin singlet state in which Cooper pairs are injected and some spin triplet states. This effect vanishes when the spin/photon coupling is equal in the two dots, due to a subradiance property caused by the entangled structure of the spin-singlets. However, realizing such an experimental scheme is challenging since it requires to couple a complex quantum dot circuit to a photonic cavity.[24–26]

The present work suggests an alternative strategy to exploit the subradiance of spin-orbit mediated transitions between spin singlet and spin-triplet CPS states. One can measure the dc current at the input of the CPS when microwave gate voltage excitations are applied separately to the two CPS dots. The microwave-induced state transitions mediated by spin-orbit coupling result in current peaks at the input of the CPS versus the dots dc gate voltages. Assuming that two on-phase microwave excitations are applied to the two dots, these peaks vanish when the amplitude of the two excitations become equal. This subradiant behavior is directly related to the spin-entanglement of the split Cooper pairs hosted by the CPS.

Note that the effects described in the present work and in Ref. 23 have the same physical origin: they both exploit spin-orbit mediated transitions between spin singlet and spin-triplet CPS states caused by the electromagnetic field. In Ref. 23, the CPS is coupled to a microwave cavity so that the electromagnetic field must be quantized in terms of the cavity photons. In the present work, no cavity is used and the electromagnetic field, which is imposed by external microwave sources, is treated classically. Nevertheless, the CPS state transitions considered in the two works are described by similar matrix elements. One important difference between the two works is that the lasing effect considered in Ref. 23 requires the CPS to lose the energy necessary for the creation of cavity photons. Therefore, all kinds of singlet/triplet transitions cannot lase: the spin singlet injected from the superconducting lead must be

higher in energy than the triplet state involved in the transition. The spectroscopic method studied in the present work allows one to probe a wider range of singlet/triplet transitions: since the microwave excitation can trigger absorption as well as emission processes, transitions in which the singlet state is lower as well as higher than the triplet state can be active.

This article is organized as follows. Section II defines the CPS hamiltonian, for a single wall carbon nanotube based implementation. Section III discusses the CPS even-charged eigenstates in the absence of the microwave excitations and without the normal metal contacts. Section IV describes the coupling between the CPS even-charged eigenstates and the microwave excitations. Section V describes the CPS state dynamics in the presence of the voltage-biased normal metal contacts, by using a master equation description. Section VI describes the results given by this approach, and, in particular, the predictions obtained for the dc current at the input of the CPS. Section VII presents further examination and modifications of the model, which are useful to put the results of Sec. VI into perspective. In particular, it discusses the role of atomic-scale disorder in the nanotube, the role of the form assumed for the spin-orbit interaction term, and possible microwave induced transitions in the CPS singly occupied charge sector. Section VIII compares the measurement strategy discussed in this work to the one of Ref. 23. Section IX concludes. Although this article focuses on a carbon-nanotube-based CPS, the entanglement detection scheme discussed in this work could be generalized to other types of quantum dots with spin-orbit coupling lik,e e.g., quantum dots made in InAs nanowires, in principle. This is briefly discussed in Sec. VII E.

II. HAMILTONIAN OF THE CPS

Let us consider the circuit represented schematically in Fig. 1. Two normal metal contacts and a superconducting

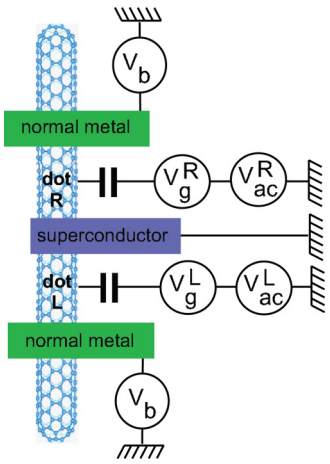

FIG. 1. (Color online) Scheme of a Cooper pair splitter made out of a carbon nanotube. The two quantum dots L and R are defined by the normal metal contacts (in green) and the superconducting contact (in blue) deposited on top of the carbon nanotube (in light blue). The dot $L(R)$ is capacitively coupled to a dc gate voltage $V_g^{L(R)}$ and microwave gate voltage $V_{\rm ac}^{L(R)}$. The superconducting contact is connected to ground and the normal metal contacts are biased with a voltage V_b.

contact are used to define two quantum dots L and R along a single wall carbon nanotube. The superconducting contact is connected to ground, and a bias voltage V_b is applied to the two normal metal contacts. The dot $L(R)$ is connected capacitively to a dc gate voltage source $V_g^{L(R)}$ and a microwave gate voltage source $V_{\rm ac}^{L(R)}(t)$. In the following, it is assumed that $V_{\rm ac}^{L}(t)$ and $V_{\rm ac}^{R}(t)$ are in phase, i.e., $V_{\rm ac}^{L(R)}(t) = v_{\rm ac}^{L(R)} \sin(\omega_{\rm RF} t)$ with $\omega_{\rm RF}$ the pulsation of the microwave excitation.

Inside the left and right dots $i \in \{L,R\}$, an electron with spin $\sigma \in \{\uparrow,\downarrow\}$ can be in the orbital $\tau \in \{K,K'\}$ of the nanotube, which is reminiscent from the K/K' degeneracy of graphene. One can use a double dot Hamiltonian that takes into account the proximity effect caused by the superconducting contact, i.e.,

$$\begin{aligned} H_{\rm DQD}^{\rm eff} = & \sum_{i,\tau,\sigma} (\varepsilon + \Delta_{\rm so}\tau\sigma) n_{i\tau\sigma} + H_{\rm prox} \\ & + \Delta_{K\leftrightarrow K'} \sum_{i,\sigma} (d_{iK\sigma}^\dagger d_{iK'\sigma} + d_{iK'\sigma}^\dagger d_{iK\sigma}) \\ & + t_{ee} \sum_{\tau,\sigma} (d_{L\tau\sigma}^\dagger d_{R\tau\sigma} + d_{R\tau\sigma}^\dagger d_{L\tau\sigma}) \end{aligned} \quad (1)$$

with

$$H_{\rm prox} = t_{\rm eh} \sum_{\tau} [(d_{L\tau\uparrow}^\dagger d_{R\bar{\tau}\downarrow}^\dagger - d_{L\bar{\tau}\downarrow}^\dagger d_{R\tau\uparrow}^\dagger) + \text{H.c.}]. \quad (2)$$

$d_{i\tau\sigma}^\dagger$ the creation operator for an electron with spin σ in orbital τ of dot $i \in \{L,R\}$ and $n_{i\tau\sigma} = d_{i\tau\sigma}^\dagger d_{i\tau\sigma}$. For simplicity, one can assume that the orbital energies in dots L and R are both equal to ε in the absence of the external microwave irradiation, which can be obtained by tuning properly the dots' dc gate voltages $V_g^{L(R)}$. The term $\Delta_{\rm so}$ is caused by spin-orbit coupling inside the carbon nanotube.[27] The term $\Delta_{K\leftrightarrow K'}$ describes a coupling between the K and K' orbitals of dot i, due to disorder at the level of the nanotube atomic structure.[27–30] The term in t_{ee} describes interdot hopping. The term $H_{\rm int}$ accounts for Coulomb charging effects. One can assume that there cannot be more than one electron in each dot, due to a strong intradot Coulomb charging energy. Therefore Cooper pairs injected inside the CPS are split into two electrons, one in each dot. The term $H_{\rm prox}$ accounts for coherent injection of singlet Cooper pairs inside the double dot.[31] This approach is valid provided quasiparticle transport between the superconducting contact and the double dot can be disregarded. This requires $eV_b < \Delta$, with Δ the BCS gap of the superconducting contact. The Hamiltonian $H_{\rm DQD}$ must be supplemented by the normal leads Hamiltonian

$$H_{\rm leads} = \sum_{k_\tau,\tau,i,\sigma} \varepsilon_{ik_\tau} c_{ik_\tau\sigma}^\dagger c_{ik_\tau\sigma} + \text{H.c.} \quad (3)$$

and the tunnel coupling between the dots and normal leads

$$H_t = \sum_{k_\tau,\tau,i,\sigma} t c_{ik_\tau\sigma}^\dagger d_{i\tau\sigma} + \text{H.c.} \quad (4)$$

with $c_{ik_\tau\sigma}$ the annihilation operator for an electron with spin σ in orbital k_τ of the normal lead $i \in \{L,R\}$.

The effect of the microwave gate voltage bias can also be described with Hamiltonian terms. The gate voltage $V_{\rm ac}^{L(R)}(t) = v_{\rm ac}^{L(R)} \sin(\omega_{\rm RF} t)$ corresponds to an electric field

$E_{\rm ac}^{L(R)} = V_{\rm ac}^{L(R)}(t)/d$, with d the center to ground separation of the waveguide providing the microwave signal. This also corresponds in the Coulomb gauge to a vector potential $A_{\rm ac}^{L(R)} = -v_{\rm ac}^{L(R)} \cos(\omega_{\rm RF} t)/\omega_{\rm RF} d$ on dot $L(R)$, which is assumed to be perpendicular to the carbon nanotube. The interplay between $A_{\rm ac}^{L(R)}$ and intersubband spin-orbit coupling elements induced by the nanotube curvature results in a spin/photon coupling term (see Ref. 32 for details)

$$H_{\rm RF}^{\rm so} = -\sum_{i,\tau,\sigma} e\alpha_{i\tau\sigma} v_{\rm ac}^{i} \cos(\omega_{\rm RF} t) d_{i\tau\sigma}^{\dagger} d_{i\tau\bar{\sigma}} \tag{5}$$

with $e > 0$ the electron charge. For simplicity, this article uses the particular structure $\alpha_{i\tau\sigma} = \mathbf{i}\sigma\alpha_i$ with $\alpha_i \in \mathbb{R}$ and $\mathbf{i}$ the imaginary unit number, obtained from a microscopic description of spin-orbit coupling in a zigzag nanotube quantum dot,[32] based on Refs. 33 and 34 (see also Refs. 35–39). However, Sec. VII A will show that the results presented here can be generalized straightforwardly to a more general $\alpha_{i\tau\sigma}$. The dimensionless coefficient α_i corresponds to the coefficient $\lambda_i/eV_{\rm rms}$ of Ref. 23, with $V_{\rm rms}$ the amplitude of vacuum voltage fluctuations for the photonic cavity considered in this reference. The value of α_i can be estimated to typically 3×10^{-4}, while $v_{\rm ac}^{L(R)}$ can reach typically 100 μV. One can also use a Hamiltonian term $H_{\rm RF}^{g}$ to account for the modulation of the dots orbital energies by the microwave gate voltages. For simplicity, one can disregard the mutual capacitive coupling between the two dots. In this case, one finds

$$H_{\rm RF}^{g} = -\sum_{i,\tau,\sigma} \kappa_i e v_{\rm ac}^{i} \sin(\omega_{\rm RF} t) n_{i\tau\sigma}, \tag{6}$$

where κ_i is a dimensionless capacitive coupling constant which is typically of the order of 10^{-2}.

In the following, it is assumed that electrons can go from dot $L(R)$ to the corresponding normal metal contact but not the reverse. This can be obtained by using a bias voltage V_b such that

$$eV_b > 2\Delta_r + t_{\rm ee} + \tfrac{1}{2}\sqrt{8t_{\rm eh}^2 + (\delta - 2\Delta_r)^2} + \lambda k_B T \tag{7}$$

with $\Delta_r = \sqrt{\Delta_{\rm so}^2 + \Delta_{K\leftrightarrow K'}^2}$ and λ a dimensionless coefficient which takes into account the effective thermal broadening of the levels (see Ref. 32 for details).

III. EXPRESSION OF THE EVEN-CHARGED CPS EIGENSTATES

This section discusses the relevant eigenstates of $H_{\rm DQD}^{\rm eff}$ in the even charge sector for $\delta \sim 2\Delta_r$, with $\delta = 2\varepsilon$ the energy of a CPS doubly occupied state for $t_{\rm eh} = \Delta_{\rm so} = \Delta_{K\leftrightarrow K'} = 0$. The parameter δ can be tuned with $V_g^{L(R)}$.

The coupling $t_{\rm eh}$ hybridizes the CPS empty state $|0,0\rangle$ with the subspace of the CPS doubly occupied states $\{|\tau\sigma,\tau'\sigma\rangle\}$, where $|\tau\sigma,\tau'\sigma\rangle$ denotes a CPS state with one electron with spin σ in orbital τ of dot L and one electron with spin σ' in orbital τ' of dot R.[40,41] The resulting even-charged subspace is called $\tilde{\mathcal{E}}$. Near the working point $\delta \sim 2\Delta_r$, the CPS dynamics involves a subspace $\mathcal{E}$ of at maximum five eigenstates from $\tilde{\mathcal{E}}$. Three of these eigenstates have an energy $E_- = \delta - 2\Delta_r$, namely,

$$|T_0\rangle = \sum_{\sigma} \frac{1}{2}\left(\sigma\frac{\Delta_{\rm so}}{\Delta_r} - 1\right)|\mathcal{C}_+(K\sigma,K'\bar{\sigma})\rangle + \frac{\Delta_{K/K'}}{2\Delta_r}\sum_{\tau}|\mathcal{C}_+(\tau\uparrow,\tau\downarrow)\rangle, \tag{8}$$

$$|T_+\rangle = \sum_{\sigma} \frac{1}{2}\left(\frac{\Delta_{\rm so}}{\Delta_r} - \sigma\right)\frac{|K\sigma,K\sigma\rangle - |K'\bar{\sigma},K'\bar{\sigma}\rangle}{\sqrt{2}} + \sum_{\sigma}\sigma\frac{\Delta_{K/K'}}{2\Delta_r}|\mathcal{C}_+(K\sigma,K'\sigma)\rangle, \tag{9}$$

and

$$|T_-\rangle = \sum_{\sigma} \frac{1}{2}\left(\frac{\Delta_{\rm so}}{\Delta_r}\sigma - 1\right)\frac{|K\sigma,K\sigma\rangle + |K'\bar{\sigma},K'\bar{\sigma}\rangle}{\sqrt{2}} + \sum_{\sigma}\frac{\Delta_{K/K'}}{2\Delta_r}|\mathcal{C}_+(K\sigma,K'\sigma)\rangle, \tag{10}$$

where $\bar{\sigma}$ denotes the spin direction opposite to σ and $|\mathcal{C}_\pm(\tau\sigma,\tau'\sigma')\rangle = (|\tau\sigma,\tau'\sigma'\rangle \pm |\tau'\sigma',\tau\sigma\rangle)/\sqrt{2}$. The two remaining eigenstates

$$|V_1\rangle = \sqrt{1 - v_1^2}|0,0\rangle + v_1|\mathcal{S}\rangle \tag{11}$$

and

$$|V_2\rangle = \sqrt{1 - v_2^2}|0,0\rangle + v_2|\mathcal{S}\rangle \tag{12}$$

have eigenenergies

$$E_{1(2)} = \tfrac{1}{2}\left[\delta - 2\Delta_r \pm \sqrt{8t_{\rm eh}^2 + (\delta - 2\Delta_r)^2}\right] \tag{13}$$

with

$$|\mathcal{S}\rangle = \sum_{\sigma}\left[\frac{1}{2}\left(\frac{\Delta_{\rm so}}{\Delta_r} - \sigma\right)|\mathcal{C}_-(K\sigma,K'\bar{\sigma})\rangle\right] + \frac{\Delta_{K/K'}}{2\Delta_r}\sum_{\tau}|\mathcal{C}_-(\tau\uparrow,\tau\downarrow)\rangle \tag{14}$$

and

$$v_{1(2)} = \frac{2t_{\rm eh}}{\sqrt{8t_{\rm eh}^2 + (\delta - 2\Delta_r)\left[\delta - 2\Delta_r \mp \sqrt{8t_{\rm eh}^2 + (\delta - 2\Delta_r)^2}\right]}}. \tag{15}$$

The existence of the K/K' degree of freedom complicates slightly the definition of the CPS eigenstates. However, from the definition of $|\mathcal{C}_\pm(\tau\sigma,\tau'\sigma')\rangle$, one can see that $|\mathcal{S}\rangle$ corresponds to a generalized spin-singlet state whereas $|T_0\rangle$, $|T_-\rangle$, and $|T_+\rangle$ correspond to generalized spin-triplet states. The coupling $t_{\rm eh}$ hybridizes the empty state $|0,0\rangle$ with $|\mathcal{S}\rangle$ only, due to the hypothesis that the superconducting contact injects spin-singlet pairs inside the CPS. Figure 2(a) shows the energies E_1, E_2, and E_- as a function of δ. The energies E_1 and E_2 show an anticrossing with a width $2\sqrt{2}t_{\rm eh}$ at $\delta = 2\Delta_r$, due to the coherent coupling between $|0,0\rangle$ and $|\mathcal{S}\rangle$. The energy E_- of the triplet states lies between E_1 and E_2. Figure 2(b) shows the transition frequencies $\omega_{V_1T_-}$, $\omega_{T_-V_2}$, and $\omega_{V_1V_2}$ of the CPS, with $\omega_{m'm} = (E_{m'} - E_m)/\hbar$. These frequencies will play an important role in the following.

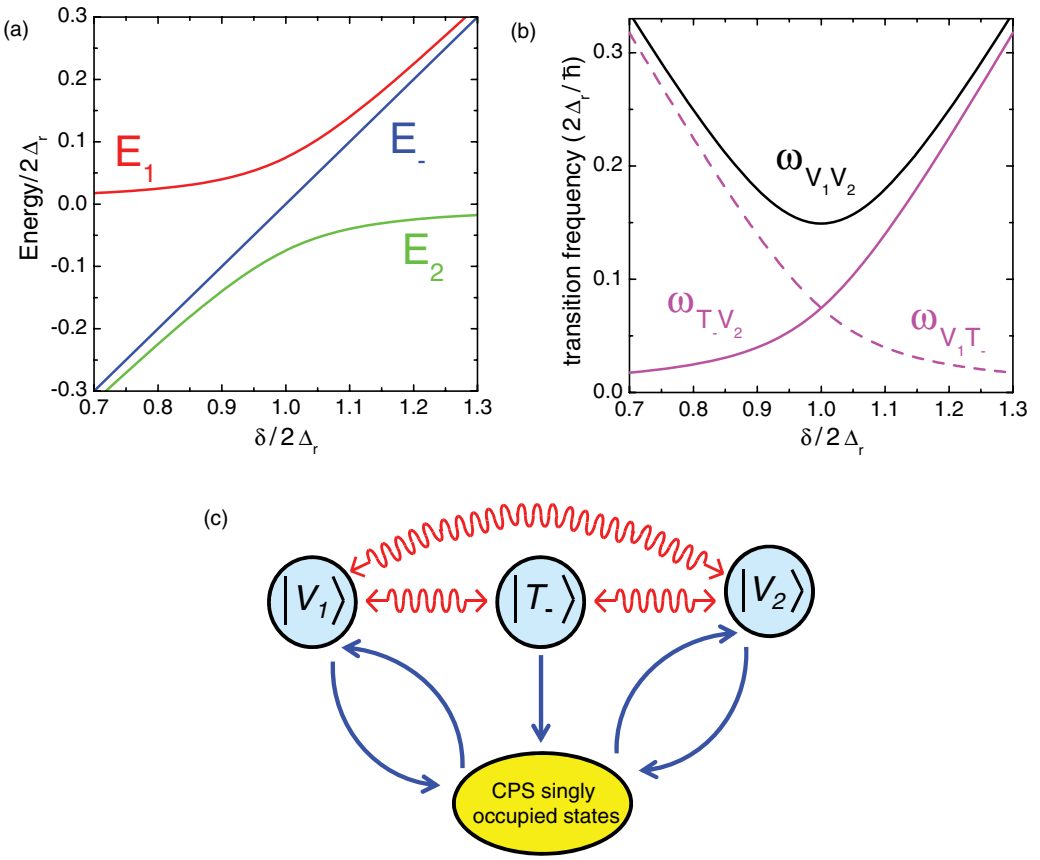

FIG. 2. (Color online) (a) Energies E_1, E_2, and E_- of the states $|V_1\rangle$, $|V_2\rangle$, and $|T_-\rangle$ as a function of δ. (b) Transition frequencies $\omega_{V_1T_-}$, $\omega_{T_-V_2}$ and $\omega_{V_1V_2}$ of the CPS as a function of δ. (c) Dynamics of the CPS near the working point $\delta = 2\Delta_r$. We consider a bias voltage regime such that the tunnel transitions between the different CPS states (blue arrows) occur together with the transfer of one electron towards the normal contacts. A microwave irradiation can induce transitions between the states $|V_1\rangle$ and $|V_2\rangle$, $|V_1\rangle$ and $|T_-\rangle$, or $|T_-\rangle$ and $|V_2\rangle$ without any transfer of electrons between the CPS and the leads (red wavy arrows). We have used $t_{\rm eh}/\Delta_{\rm so} = 1/3$ and $\Delta_{K/K'}/\Delta_{\rm so} = 6$ in (a) and (b).

IV. MICROWAVE-INDUCED MATRIX ELEMENTS

This section discusses the effect of the microwave gate bias on the eigenstates defined in Sec. III. Inside the subspace $\mathcal{E}$, $H^{\rm so}_{\rm RF}$ has only three finite matrix elements, i.e.,

$$\langle T_-|H^{\rm so}_{\rm RF}|V_{1(2)}\rangle = -\mathbf{i}ev_{1(2)}\frac{\Delta_{K\leftrightarrow K'}}{\Delta_r}\left(\alpha_L v^L_{\rm ac} - \alpha_R v^R_{\rm ac}\right)\cos(\omega_{\rm RF}t) \quad (16)$$

and

$$\langle T_+|H^{\rm so}_{\rm RF}|T_0\rangle = \mathbf{i}e\frac{\Delta_{K\leftrightarrow K'}}{\Delta_r}\left(\alpha_L v^L_{\rm ac} + \alpha_R v^R_{\rm ac}\right)\cos(\omega_{\rm RF}t). \quad (17)$$

These terms are finite because $H^{\rm so}_{\rm RF}$ flips the spins in the dots. The minus sign in Eq. (16) is a direct consequence of the fact that $|V_{1(2)}\rangle$ comprises a singlet component whereas $|T_-\rangle$ is a triplet state. In contrast, the plus sign in Eq. (17) is due to the fact that $|T_0\rangle$ and $|T_+\rangle$ are both triplet states. The matrix element of Eq. (17) is always nonresonant since it couples two states with the same energy. Therefore it can be disregarded in the present study. The Hamiltonian $H^g_{\rm RF}$ has only one finite coupling element in the subspace $\mathcal{E}$, i.e.,

$$\langle V_1|H^g_{\rm RF}|V_2\rangle = -v_1v_2e\left(\kappa_L v^L_{\rm ac} + \kappa_R v^R_{\rm ac}\right)\sin(\omega_{\rm RF}t) \quad (18)$$

with $v_1v_2 = \sqrt{2}t_{\rm eh}/\sqrt{8t^2_{\rm eh} + (\delta - 2\Delta_r)^2}$. The addition of $\kappa_L v^L_{\rm ac}$ and $\kappa_R v^R_{\rm ac}$ in Eq. (18) is due to the fact that the double occupation energy δ is shifted by $-[\kappa_L V^L_{\rm ac}(t) + \kappa_R V^R_{\rm ac}(t)]$ when a microwave excitation is applied to the device.

One can find experimental means to have $V^L_{\rm ac}$ and $V^R_{\rm ac}$ on phase, in agreement with the assumption made in Sec. II. In this case, the matrix element $\langle T_-|H^{\rm so}_{\rm RF}|V_{1(2)}\rangle$ vanishes when $\alpha_L v^L_{\rm ac} = \alpha_R v^R_{\rm ac}$. This effect is directly related to the injection of coherent singlet Cooper pairs inside the CPS since it is due to the existence of the minus sign in Eq. (16). If the injected pairs were in a product state instead of an entangled state, the matrix element (16) would not be subradiant (see Sec. VII D). Therefore coherent pair injection inside the CPS can be revealed by observing microwave-induced transitions between $|V_{1(2)}\rangle$ and $|T_-\rangle$, and checking that these transitions are suppressed for $\alpha_L v^L_{\rm ac} = \alpha_R v^R_{\rm ac}$. The following sections describe how to probe these microwave-induced transitions with a dc current measurement.

V. MASTER EQUATION DESCRIPTION OF THE CPS DYNAMICS

In the following, the states $|T_0\rangle$ and $|T_+\rangle$ are disregarded because they are not populated in simple limits where

relaxation towards them is neglected. The sequential tunneling limit $\Gamma_N \ll k_B T$ is furthermore assumed, with Γ_N the tunnel escape rate of an electron from one of the dots to the corresponding normal lead and T the temperature. For simplicity, it is assumed that this rate does not depend on the dot orbital and spin indices. This would change only quantitatively the results shown in this paper. In the absence of microwave irradiation, the dynamics of the CPS can be described with a master equation[31,42]

$$\frac{dP}{dt} = MP \tag{19}$$

with

$$P = \begin{bmatrix} P_{V_1} \\ P_{V_2} \\ P_{T_-} \\ P_{\text{single}} \end{bmatrix} \tag{20}$$

and

$$M = \begin{bmatrix} -2v_1^2\Gamma_N & 0 & 0 & (1-v_1^2)\Gamma_N \\ 0 & -2v_2^2\Gamma_N & 0 & (1-v_2^2)\Gamma_N \\ 0 & 0 & -2\Gamma_N & 0 \\ 2v_1^2\Gamma_N & 2v_2^2\Gamma_N & 2\Gamma_N & -\Gamma_N \end{bmatrix}. \tag{21}$$

Above, P_i denotes the probability of state $|i\rangle$, with $i \in \{V_1, V_2, T_-\}$. The vector P also includes the global probability P_{single} of having a double dot singly occupied state. The use of this global probability is sufficient to describe the dynamics of the CPS because the single electron tunnel rate Γ_N to the normal leads is assumed to be independent from the dot orbital and spin indices. The various singly occupied eigenstates of $H_{\text{DQD}}^{\text{eff}}$ are defined in Sec. VII C. The exact relation $v_1^2 + v_2^2 = 1$ has been used to simplify the above expression of M.

The microwave excitation $H_{\text{RF}}^{\text{so}}$ can induce resonances between the states $|V_{1(2)}\rangle$ and $|T_-\rangle$, while the excitation H_{RF}^{g} couples $|V_1\rangle$ and $|V_2\rangle$. One can use a rotating frame approximation on independent resonances to describe these effects. This approach is valid provided one of the microwave-induced resonance has a dominant effect on the others, which requires the frequencies $\omega_{V_1T_-}$, $\omega_{T_-V_2}$, and $\omega_{V_1V_2}$ to be sufficiently different. The rotating frame approximation also requires to use small amplitudes $\kappa_{L(R)}v_{\text{ac}}^{L(R)}$ and $\alpha_{L(R)}v_{\text{ac}}^{L(R)}$ compared to $\omega_{V_1T_-}$, $\omega_{T_-V_2}$, $\omega_{V_1V_2}$, and ω_{RF}. In this case, the stationary state occupation probabilities can be obtained from

$$0 = (M + M_{\text{RF}})P_{\text{stat}} \tag{22}$$

with

$$M_{\text{RF}} \tag{23}$$

$$= \begin{bmatrix} -r_{V_1T_-} - r_{V_1V_2} & r_{V_1V_2} & r_{V_1T_-} & 0 \\ r_{V_1V_2} & -r_{T_-V_2} - r_{V_1V_2} & r_{T_-V_2} & 0 \\ r_{V_1T_-} & r_{T_-V_2} & -r_{V_1T_-} - r_{T_-V_2} & 0 \\ 0 & 0 & 0 & 0 \end{bmatrix}, \tag{24}$$

$$r_{ab}(\omega) = \frac{|C_{ab}|^2}{\hbar^2} \frac{2\Gamma_{ab}}{(\omega - \omega_{ab})^2 + \Gamma_{ab}^2} > 0, \tag{25}$$

$$C_{V_1T_-} = v_1 e \frac{\Delta_{K\leftrightarrow K'}}{2\Delta_r}\left(\alpha_L v_{\text{ac}}^L - \alpha_R v_{\text{ac}}^R\right), \tag{26}$$

$$C_{T_-V_2} = v_2 e \frac{\Delta_{K\leftrightarrow K'}}{2\Delta_r}\left(\alpha_L v_{\text{ac}}^L - \alpha_R v_{\text{ac}}^R\right) \tag{27}$$

$$C_{V_1V_2} = \frac{v_1 v_2}{2} e\left(\kappa_L v_{\text{ac}}^L + \kappa_R v_{\text{ac}}^R\right), \tag{28}$$

and $\sum_i P_{\text{stat},i} = 1$. Above, Γ_{ab} corresponds to the coherence time between the states $|a\rangle$ and $|b\rangle$. Assuming that Γ_{ab} is limited by tunneling to the normal leads, one obtains $\Gamma_{V_1V_2} = \Gamma_N$, $\Gamma_{V_1T_-} = (1 + v_1^2)\Gamma_N$, and $\Gamma_{T_-V_2} = (1 + v_2^2)\Gamma_N$.

Figure 2(c) represents schematically the dynamics of the CPS near the working point $\delta = 2\Delta_r$. Due to the assumptions made in Sec. II on V_b, the tunnel transitions between the different CPS states (blue arrows) always occur together with the transfer of one electron towards one of the normal metal contacts. In contrast, the microwave irradiation induces transitions between the states $|V_1\rangle$ and $|V_2\rangle$, $|V_1\rangle$ and $|T_-\rangle$, or $|T_-\rangle$ and $|V_2\rangle$ without any exchange of electrons with the normal contacts (red wavy arrows). The state $|T_-\rangle$ can be reached through a microwave-induced transition but not through a tunnel process because it has no component in $|0,0\rangle$. The states $|V_1\rangle$ and $|V_2\rangle$ can be both reached or left through a tunnel event because they have components in both $|0,0\rangle$ and $|\mathcal{S}\rangle$.

VI. RESULTS

A. Principle of the measurement

From Eq. (21), the tunnel rate transitions from the states $|V_1\rangle$, $|V_2\rangle$, and $|T_-\rangle$ to the ensemble of the singly occupied states are $2v_1^2\Gamma_N$, $2v_2^2\Gamma_N$, and $2\Gamma_N$, respectively, while the tunnel transition rate from a singly occupied state to $|V_1\rangle$ or $|V_2\rangle$ is Γ_N. As a result, the dc current I flowing at the input of the CPS can be calculated as

$$I = R P_{\text{stat}} \tag{29}$$

with $R = e\Gamma_N[2v_1^2, 2v_2^2, 2, 1]$. Figure 3(a) shows the coefficients v_1^2 and v_2^2 as a function of δ. One can conclude from this plot that except at $\delta = 2\Delta_r$, the various components of R have different values. Therefore, a microwave excitation changing the population of the states $|V_1\rangle$, $|V_2\rangle$, and $|T_-\rangle$ should affect the value of the dc current flowing through the CPS. This effect will be used in the following to reveal the microwave-induced transitions between $|V_1\rangle$, $|V_2\rangle$, and $|T_-\rangle$.

B. Stationary CPS state occupations

Let us first discuss the dependence of the CPS state probabilities P_i on the parameter δ for $V_{\text{ac}}^{L(R)} = 0$ (see Fig. 3, black dotted lines in the three lowest panels). To understand this dependence, one must keep in mind the fact that the tunnel rate transitions from the states $|V_1\rangle$ and $|V_2\rangle$ to the ensemble of the singly occupied states are $2v_1^2\Gamma_N$ and $2v_2^2\Gamma_N$, as already discussed in Sec. VI A. For δ well below $2\Delta_r$, v_1^2 tends to zero. As a result, the CPS cannot escape easily from the state $|V_1\rangle$, whose probability tends to 1. This is because in this limit, the state $|V_1\rangle$ is almost equal to the empty state $|0,0\rangle$, which makes the emission of an electron towards the normal leads very difficult. On opposite, for δ well above $2\Delta_r$, it is the probability of the state $|V_2\rangle$ that tends to one because $|V_2\rangle$

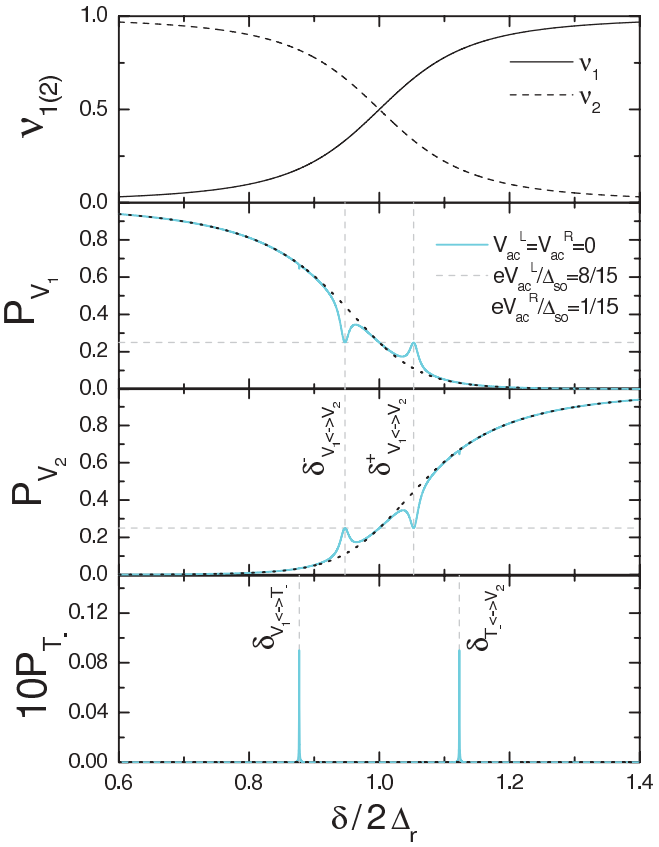

FIG. 3. (Color online) Coefficients $v^2_{1(2)}$ and probabilities P_{V_1}, P_{V_2}, and P_{T_-} of the CPS states $|V_1\rangle$, $|V_2\rangle$, and $|T_-\rangle$ as a function of δ. We have used $t_{eh}/\Delta_{so} = 1/3$, $\Delta_{K/K'}/\Delta_{so} = 3$, $2\pi\hbar\Gamma_N/\Delta_{so} = 1.37\,10^{-3}$, $ev^L_{ac}/\Delta_{so} = 1/15$, $ev^R_{ac}/\Delta_{so} = 8/15$, $\alpha_L = \alpha_R = 3.10^{-4}$, $\kappa_L = \kappa_R = 10^{-2}$, and $\omega_{RF} = 3t_{eh}$.

tends to $|0,0\rangle$. In the absence of a microwave irradiation, the probability of state $|T_-\rangle$ remains equal to zero since transitions towards these state are not possible.

Let us now discuss the case $v^{L(R)}_{ac}$ finite (see Fig. 3, red full lines in the three lowest panels). The term H^g_{RF} excites the $|V_1\rangle \leftrightarrow |V_2\rangle$ transition, which causes peaks or dips in P_{V_1} and P_{V_2} for $\omega_{RF} = \omega_{V_1V_2}$, i.e., $\delta = \delta^{\pm}_{V_1\leftrightarrow V_2}$ with

$$\delta^{\pm}_{V_1\leftrightarrow V_2} = 2\Delta_r \pm \sqrt{\omega^2_{RF} - 8t^2_{eh}}. \tag{30}$$

The term H^{so}_{RF} excites the $|V_1\rangle \leftrightarrow |T_-\rangle$ and $|T_-\rangle \leftrightarrow |V_2\rangle$ transitions, which causes peaks in P_{T_-} for $\omega_{RF} = \omega_{V_1T_-}$ and $\omega_{RF} = \omega_{T_-V_2}$, i.e., $\delta = \delta_{V_1\leftrightarrow T_-}$ and $\delta = \delta_{T_-\leftrightarrow V_2}$, respectively, with

$$\delta_{V_1\leftrightarrow T_-} = 2\Delta_r - \omega_{RF} + \left(2t^2_{eh}/\omega_{RF}\right) \tag{31}$$

and

$$\delta_{T_-\leftrightarrow V_2} = 2\Delta_r + \omega_{RF} - \left(2t^2_{eh}/\omega_{RF}\right). \tag{32}$$

The term H^{so}_{RF} also causes peaks or dips in P_{V_1} and P_{V_2}, but they are hardly visible due to the scale used in Fig. 3. The decoherence rates $\Gamma_{V_1T_-}$, $\Gamma_{T_-V_2}$ and $\Gamma_{V_1V_2}$ have similar order of magnitudes (between Γ_N and $2\Gamma_N$). However, the width of the peaks or dips caused by H^g_{RF} seems much larger than the width of the peaks caused by H^{so}_{RF}. This is due to the limit $\alpha_{L(R)} \ll \kappa_{L(R)}$ considered here. As long as the different types of resonances are well separated in frequency, the resonance $|V_1\rangle \leftrightarrow |V_2\rangle$ gives probabilities P_{V_1} and P_{V_2}, which tend to the value 1/4 for $r_{V_1V_2}$ sufficiently large. In principle, the $|V_1\rangle \leftrightarrow |T_-\rangle$ and $|T_-\rangle \leftrightarrow |V_2\rangle$ resonances give state probabilities P_i that saturate at more complicated values which depend on $v^2_{1(2)}$ when $r_{V_1T_-}$ and $r_{T_-V_2}$ become sufficiently large. In the regime $\alpha_{L(R)} \ll \kappa_{L(R)}$ considered here, the $|V_1\rangle \leftrightarrow |V_2\rangle$ resonance is saturated, while the $|V_1\rangle \leftrightarrow |T_-\rangle$ and $|T_-\rangle \leftrightarrow |V_2\rangle$ resonances are only weakly excited. This explains that the width of the peaks or dips related to the $|V_1\rangle \leftrightarrow |V_2\rangle$ resonance are much larger.

C. Average current at the input of the CPS

It is useful to discuss first the value I_0 of the current I at the input of the CPS in the absence of the microwave excitations. The current I_0 can be obtained from Eq. (29) with $v^{L(R)}_{ac} = 0$. From Fig. 4(a), I_0 shows a maximum for $\delta = 2\Delta_r$, where the two states $|V_1\rangle$ and $|V_2\rangle$ both correspond to equally weighted superpositions of $|0,0\rangle$ and $|\mathcal{S}\rangle$. For δ well below or well above $2\Delta_r$, the current I_0 vanishes because the CPS is blocked in the states $|V_1\rangle$ or $|V_2\rangle$, respectively (see Sec. V).

Figure 4(b) shows the difference between the current I for a finite microwave irradiation and I_0, as a function of ω_{RF} and δ. The $|V_1\rangle \leftrightarrow |V_2\rangle$ transitions yield a broad resonance along the curve $\omega_{RF} = \omega_{V_1V_2} = \sqrt{8t^2_{eh} + (\delta - 2\Delta_r)^2}/\hbar$, which has a frequency minimum $\omega_{RF} = 2\sqrt{2}t_{eh}/\hbar$ at $\delta - 2\Delta_r$. However, this resonance vanishes close to $\delta = 2\Delta_r$ because at this point, the tunnel escape rates $2v_1^2\Gamma_N$ and $2v_2^2\Gamma_N$ of the CPS from $|V_1\rangle$ and $|V_2\rangle$ are equal since $v_1 = v_2$ and, therefore, the microwave-induced transitions between the states $|V_1\rangle$ and $|V_2\rangle$ cannot be seen anymore through a measurement of I. The $|V_1\rangle \leftrightarrow |T_-\rangle$ and $|T_-\rangle \leftrightarrow |V_2\rangle$ resonances yield two thinner resonances which cross at the point O corresponding to $\delta = 2\Delta$ and $\hbar\omega_{RF} = \sqrt{2}t_{eh}$. For ω_{RF} tending to zero, the $|V_1\rangle \leftrightarrow |T_-\rangle(|T_-\rangle \leftrightarrow |V_2\rangle)$ resonance progressively vanishes from I because this corresponds to a regime where the state $|V_1\rangle$ ($|V_2\rangle$) is not populated anymore. Note that the calculation of the current I very close to the point O is in principle not valid using the rotating wave approximation on independent resonances since $\omega_{V_1T_-} = \omega_{T_-V_2}$ at this point. However, this represents only an extremely small area of Fig. 4(a) (of order $\Gamma_N \times \Gamma_N$). Discussing the behavior of the CPS near point O goes beyond the scope of this paper.

Figures 4(c) and 4(d) show $I - I_0$ as a function of δ for two different values of ω_{RF}. In Fig. 4(c), only the $|V_1\rangle \leftrightarrow |T_-\rangle$ and $|T_-\rangle \leftrightarrow |V_2\rangle$ resonances are visible because $\omega_{RF} < 2\sqrt{2}t_{eh}/\hbar$. In Fig. 4(d), the $|V_1\rangle \leftrightarrow |V_2\rangle$ resonances are also visible. The $|V_1\rangle \leftrightarrow |T_-\rangle$ and $|T_-\rangle \leftrightarrow |V_2\rangle$ resonances appear as much thinner an smaller peaks. At the $|V_1\rangle \leftrightarrow |V_2\rangle$ resonances, for the parameters used in Fig. 4(d), I reaches the saturation value Γ_N expected for $r_{V_1V_2}$ large and well separated resonances. This value can be obtained from Eq. (29), using $P_{stat} =^t [1/4,1/4,0,1/2]$.

D. Dependence of the CPS input current on the amplitude of the microwave irradiation

This section discusses how the minus sign in Eq. (16) can be seen experimentally. One can note $\Delta I^{\pm}_{V_1\leftrightarrow V_2} = I(\delta = \delta^{\pm}_{V_1\leftrightarrow V_2}) - I_0$, $\Delta I_{V_1\leftrightarrow T_-} = I(\delta = \delta_{V_1\leftrightarrow T_-}) - I_0$, and

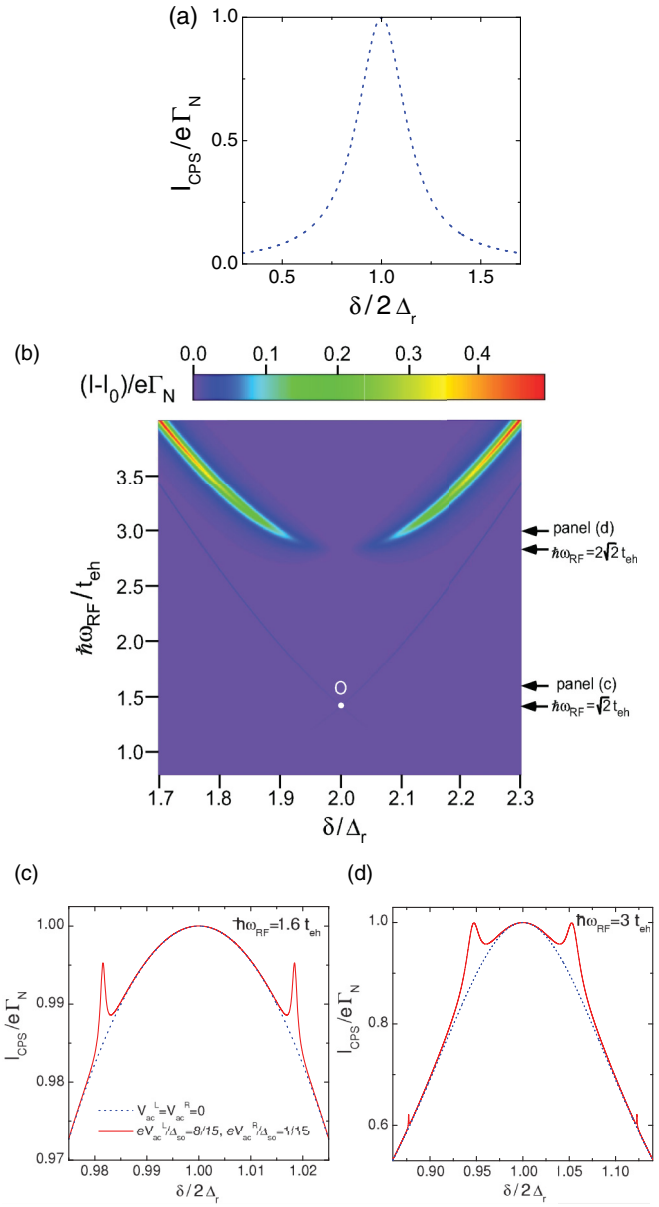

FIG. 4. (Color online) (a) Current I_0 in the absence of any microwave irradiation as a function of δ. (b) Difference between the current I for a finite microwave irradiation and the current I_0, as a function of ω_{RF} and δ. (c) and (d) Current difference $I - I_0$ as a function of δ for $\hbar\omega_{RF} = 1.6t_{eh}$ and $\hbar\omega_{RF} = 3t_{eh}$. The other parameters used are the same as in Fig. 2.

$\Delta I_{T_-\leftrightarrow V_2} = I(\delta = \delta_{T_-\leftrightarrow V_2}) - I_0$ the amplitudes of the microwave-induced current peaks appearing for $\omega_{RF} = \omega_{V_1V_2}$, $\omega_{RF} = \omega_{V_1T_-}$, and $\omega_{RF} = \omega_{T_-V_2}$. Due to the symmetries of the model around the point $\delta = 2\Delta_r$, one has $\Delta I^{\pm}_{V_1\leftrightarrow V_2} = \Delta I_{V_1\leftrightarrow V_2}$ and $\Delta I_{V_1\leftrightarrow T_-} = \Delta I_{T_-\leftrightarrow V_2}$. The top and bottom panels of Fig. 5 show the variations of $\Delta I_{V_1\leftrightarrow T_-}$ and $\Delta I_{V_1\leftrightarrow V_2}$ with v_{ac}^R for a constant value of v_{ac}^L. Due to the plus sign in Eq. (18), $\Delta I_{V_1\leftrightarrow V_2}$ increases monotonically with v_{ac}^L. In Fig. 5, this variation is very small because the $|V_1\rangle \leftrightarrow |V_2\rangle$ resonance is already saturated at $v_{ac}^R = 0$ due to the value used for v_{ac}^L. In contrast, due to the minus sign in Eq. (16), $\Delta I_{V_1\leftrightarrow T_-}$ shows a minimum for $v_{ac}^L = v_{ac}^R$. Note that if the electrons pairs injected in the

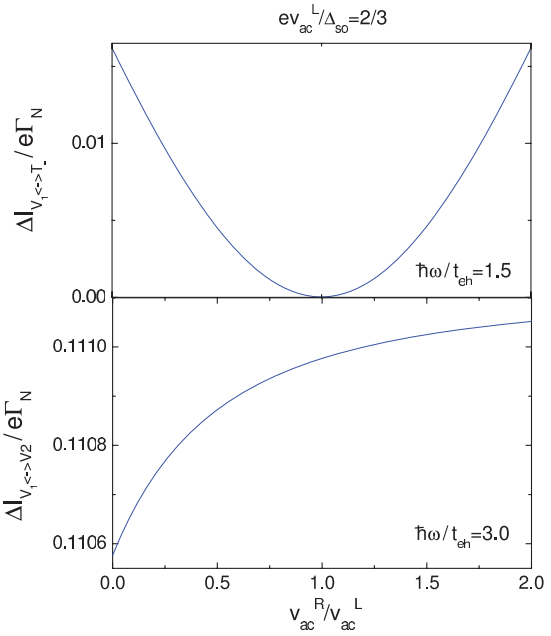

FIG. 5. (Color online) Amplitude of the current peaks $\Delta I_{V_1\leftrightarrow T_-}$ (top panel) and $\Delta I_{V_1\leftrightarrow V_2}$ (bottom panel) as a function of v_{ac}^R for a constant value of v_{ac}^L, i.e., $ev_{ac}^L/\Delta_{so} = 2/3$. The other parameters used are the same as in Fig. 2.

CPS were not in an entangled state but in a product state, such a nonmonotonic behavior would not be possible. For the parameters considered in Fig. 5, top panel, $\Delta I_{V_1\leftrightarrow T_-}$ vanishes at $v_{ac}^L = v_{ac}^R$ because the effects of the $|V_1\rangle \leftrightarrow |V_2\rangle$ resonance can be disregarded. This should not be true anymore in the case where the different types of resonances are not well separated, which can happen, e.g., if t_{eh} is too small with respect to the width of the resonances. However, in this case, one can still expect $\Delta I_{V_1\leftrightarrow T_-}$ to show a strongly nonmonotonic behavior with a minimum at $v_{ac}^L = v_{ac}^R$, provided the couplings $\alpha_{L(R)}$ are sufficiently strong. Treating this case requires to go beyond the rotating frame approximation with independent resonances used in this work.

E. Experimental parameters

This section discusses the parameters used in the Figures and the order of magnitude of the signals which can be expected in practice. In Figs. 3 to 5, the ratio of parameters used correspond for instance to realistic values $t_{eh} = 50\ \mu$eV (see Refs. 7–11), $\Delta_{so} = 0.15$ meV, $\Delta_{K/K'} = 0.45$ meV, and $\Gamma_N = 50$ MHz (see Refs. 27–29). Note that $\Gamma_N = 50$ MHz corresponds to 6.5 mK, therefore the sequential tunneling approximation used in this work is valid using for instance $T = 65$ mK. In this case, using $\lambda = 5$, the condition (7) to have electrons flowing only from the dot to the leads and not the reverse gives $V_b > 1.05$ mV (see Sec. II). This is compatible with the condition $V_b < \Delta$ for having no quasiparticle transport between the superconducting lead and the dots, by using for instance a Nb contact for which $\Delta \simeq 1.4$ meV or a NbN contact for which $\Delta \simeq 3$ meV. Using the above parameters, the ratio $v_{ac}^{L(R)}/\Delta_{so}$ used in Figs. 3 and 4 corresponds to realistic microwave amplitudes

$v_{\rm ac}^L = 10\,\mu$V and $v_{\rm ac}^R = 80\,\mu$V. Besides, the maximum frequency $\omega_{\rm RF} = 4t_{\rm eh}$ considered in this work [see Fig. 4(b)] corresponds to 48.5 GHz, and the frequency at point O corresponds to 17 GHz, which is accessible with current microwave technologies.[43] Using the above parameters, the amplitude of the current peaks $\Delta I_{V_1\leftrightarrow V_2}$ and $\Delta I_{V_1\leftrightarrow T_-}$ shown in Fig. 3(d) are $\Delta I_{V_1\leftrightarrow V_2} = 884$ fA and $\Delta I_{V_1\leftrightarrow T_-} = 207$ fA over a background I_0 of 7.1 and 4.8 pA, respectively. The maximum current difference $\Delta I_{V_1\leftrightarrow T_-}$ in Fig. 5, top panel, corresponds to 129 fA for a background of 8 pA. Therefore the features described in this article seem measurable experimentally.

VII. DISCUSSION ON THE SPECTROSCOPIC ENTANGLEMENT DETECTION SCHEME

The present section presents further examination and modifications of the model used above, in order to put the results of Sec. VI into perspective.

A. Use of a more general spin/orbit coupling term

The $H_{\rm RF}^{\rm so}$ coupling term of Eq. (5) accounts for the coupling between the CPS and microwave excitations mediated by spin-orbit coupling. The above sections have used the particular form $\alpha_{i\tau\sigma} = \mathbf{i}\sigma\alpha_i$ with $\alpha_i \in \mathbb{R}$, obtained from a microscopic description of spin-orbit coupling in a zigzag nanotube quantum dot.[32] This section discusses the generalization of the results to a more general coupling $\alpha_{i\tau\sigma}$. Since $H_{\rm RF}^{\rm so}$ must be Hermitian, one can use $\alpha_{i\tau\uparrow} = \alpha_{i\tau}$ and $\alpha_{i\tau\downarrow} = \alpha_{i\tau}^*$ without any loss of generality. The parameter

$$|\Delta\alpha|e^{\mathbf{i}\varphi_\alpha} = (\alpha_{LK} + \alpha_{LK'})v_{\rm ac}^L - (\alpha_{RK} + \alpha_{RK'})v_{\rm ac}^R \quad (33)$$

with $\varphi_\alpha \in]-\pi,\pi]$ plays a crucial role in this case. It is convenient to redefine the states $|T_+\rangle$ and $|T_-\rangle$ more generally as

$$|T_+\rangle = \mathbf{i}\,\mathrm{sgn}(\varphi_\alpha)(e^{-\mathbf{i}\varphi_\alpha}|\tilde{T}_\uparrow\rangle + e^{\mathbf{i}\varphi_\alpha}|\tilde{T}_\downarrow\rangle)/\sqrt{2} \quad (34)$$

and

$$|T_-\rangle = \mathbf{i}\,\mathrm{sgn}(\varphi_\alpha)(e^{-\mathbf{i}\varphi_\alpha}|\tilde{T}_\uparrow\rangle - e^{\mathbf{i}\varphi_\alpha}|\tilde{T}_\downarrow\rangle)/\sqrt{2} \quad (35)$$

with

$$|\tilde{T}_\sigma\rangle = \frac{1}{2}\left(\sigma\frac{\Delta_{\rm so}}{\Delta_r} - 1\right)|K\sigma,K\sigma\rangle - \frac{1}{2}\left(1 + \sigma\frac{\Delta_{\rm so}}{\Delta_r}\right)|K'\sigma,K'\sigma\rangle + \frac{\Delta_{K/K'}}{2\Delta_r}(|K\sigma,K'\sigma\rangle + |K'\sigma,K\sigma\rangle). \quad (36)$$

Note that $|T_+\rangle$ and $|T_-\rangle$ are still eigenstates of the Hamiltonian $H_{\rm DQD}^{\rm eff}$, with energy $\delta - 2\Delta_r$, corresponding to generalized spin-triplet states. The definitions of the other states $|V_{1(2)}\rangle$ and $|T_0\rangle$ remain unchanged. Using expressions (34) and (35), one obtains

$$\langle T_+|H_{\rm RF}^{\rm so}|V_{1(2)}\rangle = 0 \quad (37)$$

and

$$\langle T_-|H_{\rm RF}^{\rm so}|V_j\rangle = -\mathbf{i}ev_j\frac{\Delta_{K\leftrightarrow K'}}{2\Delta_r}|\Delta\alpha|\mathrm{sgn}(\varphi_\alpha)\cos(\omega_{\rm RF}t) \quad (38)$$

for $j \in \{1,2\}$. In Secs. II to VI, one uses $\alpha_{i\tau} = \mathbf{i}\alpha_i$ thus $\varphi_\alpha = \mathrm{sgn}(\alpha_L - \alpha_R)\pi/2$ and $|T_\pm\rangle = (|\tilde{T}_\uparrow\rangle \mp |\tilde{T}_\downarrow\rangle)/\sqrt{2}$ which is in agreement with Eqs. (9) and (10). In this limit, Eq. (38) agrees with Eq. (16). Equations (38) and (33) show that even with a more general coupling term $H_{\rm RF}^{\rm so}$, the matrix elements $\langle T_-|H_{\rm RF}^{\rm so}|V_{1(2)}\rangle$ still present a subradiant form. Hence, the entanglement detection scheme discussed in this article appears to be quite general. Using a more general $H_{\rm RF}^{\rm so}$ will modify only quantitatively the predictions of Sec. VI.

B. Role of $\Delta_{K\leftrightarrow K'} \neq 0$

Remarkably, the subradiant matrix elements (16) and (38) vanish for $\Delta_{K\leftrightarrow K'} = 0$. The aim of the present section is to show that using a finite $\Delta_{K\leftrightarrow K'}$ does not represent a fundamental constraint to have the subradiance effect. Indeed, $|V_{1(2)}\rangle$ can still be coupled to other triplet states outside of the subspace $\mathcal{E}$ when $\Delta_{K\leftrightarrow K'} = 0$. This fact is illustrated below, using $\alpha_{i\tau} = \mathbf{i}\alpha_i$ for simplicity. In this case, $|V_{1(2)}\rangle$ is coupled to a single triplet eigenstate $|T_b\rangle$ of $H_{\rm DQD}^{\rm eff}$ outside the subspace $\mathcal{E}$, defined by

$$|T_b\rangle = \frac{\alpha_-(|\tilde{T}_{1\uparrow}\rangle - |\tilde{T}_{2\downarrow}\rangle)}{\sqrt{2(\alpha_-^2 + \alpha_+^2)}} - \frac{\alpha_+(|\tilde{T}_{2\uparrow}\rangle - |\tilde{T}_{1\downarrow}\rangle)}{\sqrt{2(\alpha_-^2 + \alpha_+^2)}} \quad (39)$$

with

$$|\tilde{T}_{1\sigma}\rangle = \frac{\Delta_{K/K'}}{2\tilde{\Delta}_r}(|K'\sigma,K'\sigma\rangle - |K\sigma,K\sigma\rangle) + \sigma\frac{\Delta_{\rm so}}{\tilde{\Delta}_r}|K'\sigma,K\sigma\rangle, \quad (40)$$

$$|\tilde{T}_{2\sigma}\rangle = \frac{\Delta_{K/K'}}{2\tilde{\Delta}_r}(|K'\sigma,K'\sigma\rangle - |K\sigma,K\sigma\rangle) + \sigma\frac{\Delta_{\rm so}}{\tilde{\Delta}_r}|K\sigma,K'\sigma\rangle \quad (41)$$

$$\alpha_\pm = \tilde{\alpha}_L - \tilde{\alpha}_R \pm \frac{\Delta_{\rm so}}{\Delta_r}(\tilde{\alpha}_L + \tilde{\alpha}_R), \quad (42)$$

and

$$\tilde{\alpha}_{L(R)} = \alpha_{L(R)}v_{\rm ac}^{L(R)}, \quad (43)$$

such that

$$H_{\rm DQD}^{\rm eff}|T_b\rangle = \delta\,|T_b\rangle\,. \quad (44)$$

One can check that

$$\langle T_b|h_{\rm so}|V_{1(2)}\rangle = \mathbf{i}ev_{1(2)}\frac{\Delta_{\rm so}^2}{\Delta_r}(\tilde{\alpha}_R^2 - \tilde{\alpha}_L^2)\cos(\omega_{\rm RF}t) \times\sqrt{\Delta_{\rm so}^2(\tilde{\alpha}_L^2 + \tilde{\alpha}_R^2) + \frac{\Delta_{K/K'}^2}{2}(\tilde{\alpha}_L - \tilde{\alpha}_R)^2}. \quad (45)$$

For $\Delta_{K\leftrightarrow K'} \to 0$, one finds

$$\langle T_b|h_{\rm so}|V_{1(2)}\rangle = \mathbf{i}e\frac{v_{1(2)}(\tilde{\alpha}_L^2 - \tilde{\alpha}_R^2)}{\sqrt{\tilde{\alpha}_L^2 + \tilde{\alpha}_R^2}}\cos(\omega_{\rm RF}t). \quad (46)$$

The coupling between $|V_{1(2)}\rangle$ and $|T_b\rangle$ is subradiant since it vanishes for $\alpha_R v_{\rm ac}^R = \alpha_L v_{\rm ac}^L$. Nevertheless, for realistic parameters and, in particular, $\Delta_r \gg t_{\rm eh}$, the transition frequencies $\omega_{T_bV_1}$ and $\omega_{T_bV_1}$ correspond approximately to $2\Delta_r/\hbar$, which is too high for current microwave technology. This is why this paper focuses on microwave-induced transitions inside the subspace $\mathcal{E}$.

C. Microwave-induced transitions inside the singly occupied charge sector

The different eigenstates of $H_{\rm DQD}^{\rm eff}$ in the singly occupied charge sector can be defined as

$$|b_{1\sigma}\rangle = \frac{1}{2}\sqrt{1-\sigma\frac{\Delta_{\rm so}}{\Delta_r}}(|K\sigma,0\rangle - |0,K\sigma\rangle) + \frac{\Delta_{K/K'}}{2\Delta_r\sqrt{1-\sigma\frac{\Delta_{\rm so}}{\Delta_r}}}(|0,K'\sigma\rangle - |K'\sigma,0\rangle), \quad (47)$$

$$|a_{1\sigma}\rangle = -\frac{1}{2}\sqrt{1-\sigma\frac{\Delta_{\rm so}}{\Delta_r}}(|K\sigma,0\rangle + |0,K\sigma\rangle) + \frac{\Delta_{K/K'}}{2\Delta_r\sqrt{1-\sigma\frac{\Delta_{\rm so}}{\Delta_r}}}(|0,K'\sigma\rangle + |K'\sigma,0\rangle), \quad (48)$$

$$|b_{2\sigma}\rangle = -\frac{1}{2}\sqrt{1+\sigma\frac{\Delta_{\rm so}}{\Delta_r}}(|K\sigma,0\rangle - |0,K\sigma\rangle) + \frac{\Delta_{K/K'}}{2\Delta_r\sqrt{1+\sigma\frac{\Delta_{\rm so}}{\Delta_r}}}(|0,K'\sigma\rangle - |K'\sigma,0\rangle), \quad (49)$$

and

$$|a_{2\sigma}\rangle = \frac{1}{2}\sqrt{1+\sigma\frac{\Delta_{\rm so}}{\Delta_r}}(|K\sigma,0\rangle + |0,K\sigma\rangle) + \frac{\Delta_{K/K'}}{2\Delta_r\sqrt{1+\sigma\frac{\Delta_{\rm so}}{\Delta_r}}}(|0,K'\sigma\rangle + |K'\sigma,0\rangle) \quad (50)$$

for $\sigma \in \{\uparrow,\downarrow\}$. These states have eigenenergies ε_1^b, ε_1^a, ε_2^b, and ε_2^a, respectively, with

$$\varepsilon_i^b = \varepsilon - t_{\rm ee} + (-1)^i\Delta_r \quad (51)$$

and

$$\varepsilon_i^a = \varepsilon + t_{\rm ee} + (-1)^i\Delta_r \quad (52)$$

for $i \in \{1,2\}$. The states $|b_{1\sigma}\rangle$ and $|b_{2\sigma}\rangle$ can be seen as generalized bonding states and $|a_{1\sigma}\rangle$ and $|a_{2\sigma}\rangle$ as generalized antibonding states. This section uses $\alpha_{i\tau} = \mathbf{i}\alpha_i$ for simplicity. The term $H_{\rm RF}^{\rm so}$ couples $|b_{i\sigma}\rangle$ and $|a_{i\sigma}\rangle$ to $|b_{i\overline{\sigma}}\rangle$ and $|a_{i\overline{\sigma}}\rangle$ only, for $i \in \{1,2\}$. Only the transitions $|a_{i\sigma}\rangle \leftrightarrow |b_{i\overline{\sigma}}\rangle$ correspond to a finite frequency, i.e., $\omega_{a_{i\sigma}b_{i\overline{\sigma}}} = 2t_{\rm ee}/\hbar$. One can check that

$$\langle b_{i\overline{\sigma}}|H_{\rm RF}^{\rm so}|a_{i\sigma}\rangle = -\mathbf{i}e\left(\alpha_L v_{\rm ac}^L - \alpha_R v_{\rm ac}^R\right)\cos(\omega_{\rm RF}t)/2, \quad (53)$$

whereas

$$\langle b_{i\overline{\sigma}}|H_{\rm RF}^{\rm so}|b_{i\sigma}\rangle = \langle a_{i\overline{\sigma}}|H_{\rm RF}^{\rm so}|a_{i\sigma}\rangle = \mathbf{i}e\left(\alpha_L v_{\rm ac}^L + \alpha_R v_{\rm ac}^R\right)\cos(\omega_{\rm RF}t)/2. \quad (54)$$

Importantly, the matrix element of Eq. (53) has a subradiant structure. This property is due to the fact that the states $|b_{i\overline{\sigma}}\rangle$ and $|a_{i\sigma}\rangle$ are entangled states with different symmetries, i.e., $|b_{i\overline{\sigma}}\rangle$ is an antibonding state that contains some $|\tau\overline{\sigma},0\rangle + |0,\tau\overline{\sigma}\rangle$ components, whereas $|a_{i\sigma}\rangle$ is a bonding state that contains $|\tau\sigma,0\rangle - |0,\tau\sigma\rangle$ components. This is analogous to the fact that the elements $\langle T_-|H_{\rm RF}^{\rm so}|V_j\rangle$ couple a state $|V_j\rangle$ with a spin-singlet component to a spin-triplet state $|T_-\rangle$. In contrast, the matrix elements of Eq. (54) are not subradiant because they couple two entangled states with similar symmetries, i.e., two bonding or two antibonding states.

Due to the subradiant form of Eq. (53), the transitions $|a_{i\sigma}\rangle \leftrightarrow |b_{i\overline{\sigma}}\rangle$ can lead to a non-monotonic variation of the CPS input current as a function of, e.g., $v_{\rm ac}^L$, due to another type of entanglement than the one discussed in Sec. VI. Therefore, in the context of the characterization of split Cooper pairs entanglement, one needs to find a way to discriminate possible current resonances corresponding to the transitions $|a_{i\sigma}\rangle \leftrightarrow |b_{i\overline{\sigma}}\rangle$ and $|V_{1(2)}\rangle \leftrightarrow \langle T_-|$. In practice, this should be feasible by studying how the different resonance frequencies vary with the DC gate voltages of the two dots. Indeed, $\omega_{a_{i\sigma}b_{i\overline{\sigma}}}$ does not depend on the parameter δ, contrarily to $\omega_{V_1T_-}$ and $\omega_{T_-V_2}$. Therefore possible current resonances due to $|a_{i\sigma}\rangle \leftrightarrow |b_{i\overline{\sigma}}\rangle$ transitions should appear as horizontal lines in Fig. 4(b). This effect was nevertheless disregarded in Sec. VI, assuming that $\omega_{a_{i\sigma}b_{i\overline{\sigma}}}$ is too large to be accessible experimentally. Studying quantitatively the possibility to observe the resonances $|a_{i\sigma}\rangle \leftrightarrow |b_{i\overline{\sigma}}\rangle$ requires to go beyond the approximation of an electronic tunnel rate Γ_N to the normal leads which is independent from the dot orbital and spin indices.[44]

D. Simplified model without the K/K' degeneracy

It is interesting to discuss a model without the K/K' degree of freedom to show simply how the subradiance property arises.

1. Case of coherent Cooper pair injection

Let us assume that each of the two CPS dots has a single orbital. One can note $|\sigma,\sigma'\rangle$ a CPS doubly occupied state with a spin $\sigma(\sigma')$ on dot $L(R)$. In the case of coherent Cooper pair injection, the double quantum dot effective Hamiltonian can be written[31]

$$H_{\rm DQD}^{\rm eff} = \varepsilon(n_{L\sigma} + n_{R\sigma}) + (t_{\rm eh}/\sqrt{2})(d_{L\uparrow}^\dagger d_{R\downarrow}^\dagger - d_{L\downarrow}^\dagger d_{R\uparrow}^\dagger + \text{H.c.}) + H_{\rm int}, \quad (55)$$

where $H_{\rm int}$ still forbids the double occupation of each dot. One uses above $n_{i\sigma} = d_{i\sigma}^\dagger d_{i\sigma}$ with $d_{i\sigma}^\dagger$ the creation operator for an electron with spin σ in dot $i \in \{L,R\}$. Let us furthermore assume that there also exists a spin-flip coupling term to the microwave signal with the form

$$H_{\rm RF}^{sf} = -\sum_i \alpha_i e v_{\rm ac}\cos(\omega_{\rm RF}t)(d_{i\uparrow}^\dagger d_{i\downarrow} + d_{i\downarrow}^\dagger d_{i\uparrow}) = \sum_i \lambda_i(d_{i\uparrow}^\dagger d_{i\downarrow} + d_{i\downarrow}^\dagger d_{i\uparrow}). \quad (56)$$

Such a spin-flip coupling can be due for instance to the magnetic field associated with the microwave irradiation. In practice, this term should have a very weak amplitude, but it is nevertheless discussed here for fundamental purposes.

The term in $t_{\rm eh}$ hybridizes the CPS empty state $|0,0\rangle$ with the singlet state $|\tilde{\mathcal{S}}\rangle = (|\uparrow,\downarrow\rangle - |\downarrow,\uparrow\rangle)/\sqrt{2}$, so that an anticrossing appears again in the spectrum of the CPS even-charged states. For simplicity, it is asssumed below that the double occupation energy $\delta = 2\varepsilon$ of the CPS is degenerate with the energy of $|0,0\rangle$, i.e., $\delta = 0$. In this case, one can use the orthonormalized basis $\mathcal{A} = \{\tilde{V}_1,\tilde{V}_2,|\tilde{T}_a\rangle,|\tilde{T}_b\rangle,|\tilde{T}_0\rangle\}$ of eigenstates of Eq. (55) in

the even charge sector with

$$|\tilde{V}_{1(2)}\rangle = (|0,0\rangle \pm |\tilde{S}\rangle)/\sqrt{2}, \quad (57)$$

$$|\tilde{T}_{a(b)}\rangle = (|\uparrow,\uparrow\rangle \pm |\downarrow,\downarrow\rangle)/\sqrt{2}, \quad (58)$$

and

$$|\tilde{T}_0\rangle = (|\uparrow,\downarrow\rangle + |\downarrow,\uparrow\rangle)/\sqrt{2}. \quad (59)$$

The states $|\tilde{V}_1\rangle$ and $|\tilde{V}_2\rangle$ have energies $\tilde{E}_1$ and $\tilde{E}_2$ given by $\tilde{E}_{1(2)} = \pm t_{\rm eh}$. They play the role of the states $|V_1\rangle$ and $|V_2\rangle$ of Sec. VI. It is convenient to define $|\tilde{T}_a\rangle$ and $|\tilde{T}_b\rangle$ as superpositions of triplet states with equal spins. The states $|\tilde{T}_0\rangle$, $|\tilde{T}_a\rangle$, and $|\tilde{T}_b\rangle$ have an energy $\delta = 0$. One can check straigthforwardly that

$$H_{\rm RF}^{sf}|\tilde{S}\rangle = (\lambda_R - \lambda_L)|\tilde{T}_b\rangle, \quad (60)$$

thus

$$\langle\tilde{T}_b|H_{\rm RF}^{sf}|\tilde{V}_{1(2)}\rangle = \pm(\lambda_R - \lambda_L)/\sqrt{2}, \quad (60)$$

whereas $\langle\tilde{T}_{a(0)}|H_{\rm RF}^{sf}|\tilde{V}_{1(2)}\rangle = 0$ and $\langle\tilde{V}_2|H_{\rm RF}^{sf}|\tilde{V}_1\rangle = 0$. The states $\tilde{V}_{1(2)}$ are thus coupled by $H_{\rm RF}^{sf}$ to a single state $|\tilde{T}_b\rangle$, with a subradiant matrix element (60). This illustrates the universality of the mechanism discussed in Sec. VI.

2. *Case of incoherent singlet injection*

One can model naively the incoherent injection of Cooper pairs inside the CPS by assuming that up spins are always injected inside the left dot and right spins inside the right dot. This requires to replace the Hamiltonian (55) by

$$H_{\rm DQD}^{\rm eff} = \varepsilon(n_{L\sigma} + n_{R\sigma}) + t_{\rm eh}(d_{L\uparrow}^{\dagger}d_{R\downarrow}^{\dagger} + d_{R\downarrow}d_{L\uparrow}) + H_{\rm int}. \quad (61)$$

One can use again $\delta = 2\varepsilon = 0$ for simplicity. In this case, one can define an orthonormalized basis $\mathcal{B} = \{W_1, W_2, |\tilde{T}_c\rangle, |\tilde{T}_d\rangle, |\tilde{T}_e\rangle\}$ of eigenstates of Eq. (61) in the even charge sector, with

$$|W_{1(2)}\rangle = (|0,0\rangle \pm |\uparrow,\downarrow\rangle)/\sqrt{2}, \quad (62)$$

$$|\tilde{T}_c\rangle = (\lambda_R|\uparrow,\uparrow\rangle + \lambda_L|\downarrow,\downarrow\rangle)/\sqrt{\lambda_L^2 + \lambda_R^2}, \quad (63)$$

$$|\tilde{T}_d\rangle = (\lambda_L|\uparrow,\uparrow\rangle - \lambda_R|\downarrow,\downarrow\rangle)/\sqrt{\lambda_L^2 + \lambda_R^2}, \quad (64)$$

and $|\tilde{T}_e\rangle = |\downarrow,\uparrow\rangle$. The role of the states $|V_1\rangle$ and $|V_2\rangle$ of Sec. VI is now played by $|W_1\rangle$ and $|W_2\rangle$. The states $|W_1\rangle$ and $|W_2\rangle$ have again energies $\tilde{E}_1$ and $\tilde{E}_2$ defined in the previous section, whereas the states $|\tilde{T}_c\rangle$, $|\tilde{T}_d\rangle$, and $|\tilde{T}_e\rangle$ have an energy $\delta = 0$. The states $|\tilde{T}_a\rangle$ and $|\tilde{T}_b\rangle$ of the previous section are still CPS eigenstates, but it is more convenient to use the eigenstates $|\tilde{T}_c\rangle$ and $|\tilde{T}_d\rangle$ to study the effect of $H_{\rm RF}^{sf}$. Due to the term in $t_{\rm eh}$, the states $|W_1\rangle$ and $|W_2\rangle$ still form an anticrossing in the energy spectrum of the CPS. Hence, such an anticrossing is not characteristic from the injection of entangled Cooper pairs. The only state of $\mathcal{B}$ connected to $|W_{1(2)}\rangle$ by $H_{\rm RF}^{sf}$ is $|\tilde{T}_c\rangle$, with a matrix element

$$\langle\tilde{T}_c|H_{\rm RF}^{sf}|W_{1(2)}\rangle = \pm\sqrt{2\left(\lambda_L^2 + \lambda_R^2\right)}, \quad (65)$$

which is not subradiant, but increases monotonically with λ_R and λ_L. Therefore the subradiance property is lost when Cooper pairs are injected inside the CPS in a product state instead of an entangled state. Similar results are expected for a model including the K/K' degree of freedom. This illustrates that the subradiance property is a good indication of the injection of entangled Cooper pairs inside the CPS. More sophisticated descriptions of incoherent injection of Cooper pairs into the CPS are beyond the scope of this article.

E. Case of a CPS made from an InAs nanowire

This article mainly discusses the case of a carbon-nanotube based CPS, in which quantum dots present a twofold orbital degeneracy. However, semiconducting nanowires can also be used to fabricate a CPS. In particular, Refs. 7–9 and 12 have used InAS nanowires. Quantum dots fabricated in InAS nanowires do not present an orbital degeneracy. Therefore, in proper biasing conditions, one can consider that, for each dot of the CPS, only a single orbital participates to current transport. If there is no magnetic field, no spin-orbit coupling and no contacts, one can consider that each dot has two eigenstates: the spin-up and the spin-down states, which are degenerate and form a Kramers doublet. Now, if a finite spin-orbit coupling exists, the Kramers doublet remains degenerate in the absence of a magnetic field, because spin-orbit coupling alone cannot lift time reversal symmetry. This implies that the two spin states remain uncoupled. It is necessary to use a finite magnetic field to obtain an electric-field controlled coupling of the spins states mediated by the spin-orbit interaction, as explained in Ref. 45. Following Ref. 45, the amplitude of this coupling is set by a constant that has the same order of magnitude as the coefficients $\alpha_{L(R)}$ introduced in Sec. II. Therefore, in principle, singlet/triplet resonances similar to those studied in this article could occur with an InAs-nanowire-based CPS. In order to study quantitatively such an effect with a minimal single orbital model, one can generalize straightforwardly the single-orbital model of Sec. VII D to the case of a lifted spin degeneracy. This will not be discussed here.

VIII. COMPARISON WITH AN ALTERNATIVE SETUP: THE CPS EMBEDDED IN A MICROWAVE CAVITY

This section compares the experimental scheme proposed in Ref. 23 to the scheme discussed in the present article. Reference 23 suggests to insert the CPS inside a coplanar microwave cavity. In this case, the electromagnetic field coupled to the CPS can be quantized in terms of the cavity photons. Nevertheless, the CPS state transitions considered in Ref. 23 and in the present work are described by similar matrix elements. When a microwave cavity is used, the minus sign in Eq. (16) can be observed through a lasing effect involving the $|V_1\rangle \rightarrow |T_-\rangle$ transition. This minus sign leads to a nonmonotonic dependence of the number of photons in the cavity as a function of the coefficients α_L and α_R, which mediate a coupling between the CPS and the electric field conveyed by the cavity. Since this electric field can be considered as constant over the whole CPS area, it is necessary to be able to vary α_L independently from α_R to observe a nonmonotonic variation of the number of photons. This can require to complexify the CPS design, for instance. In the present scheme, such a control on α_L and α_R is not necessary since

it is sufficient to vary independently the amplitudes v_{ac}^{L} and v_{ac}^{R}. This can be naturally achieved by using two independent microwave supplies for the two gates. The advantage of the scheme presented in Ref. 23 is that the signal to be measured is a large photon number that can be obtained by measuring the power spectrum emitted by the cavity. In other words, the scheme of Ref. 23 exploits the fact that the lasing effect provides an intrinsic amplification process for the $|V_1\rangle \rightarrow |T_-\rangle$ transitions. In the present scheme, the measurement seems a bit more difficult since the current peaks to be measured are very small. Nevertheless, such current amplitudes are measurable, in principle.[43] Therefore the scheme presented in this reference could be an interesting alternative approach to demonstrate the coherent injection of singlet Cooper pairs inside a CPS. This scheme, furthermore, allows one to study also the $|V_2\rangle \leftrightarrow \langle T_-|$ transition, which is not possible with the scheme of Ref. 23. Indeed, the lasing effect requires the CPS to lose the energy necessary for the creation of cavity photons. The $|V_2\rangle \leftrightarrow \langle T_-|$ transition cannot be involved in a lasing effect because $\langle T_-|$ has a higher energy than the state $|V_2\rangle$ initially populated due to the injection of Cooper pairs. More generally, the spectroscopic method considered in the present work allows one to probe a wider range of singlet/triplet transitions because the microwave excitation can trigger absorption as well as emission processes.

IX. CONCLUSION

The dc current response of a double-quantum-dot based CPS to a microwave gate irradiation is a very rich source of information on Cooper pair splitting. In particular, it can reveal the entanglement of spin-singlet Cooper pairs injected inside the CPS. This article illustrates this property for a double quantum dot formed inside a carbon nanotube with typical parameters. If they are spin-entangled, the injected pairs are coupled to other CPS states through some subradiant microwave transitions mediated by spin-orbit coupling. This property can be revealed by applying to the two CPS quantum dots two on-phase microwave gate voltages. The spin-orbit mediated microwave transitions cause dc current resonances at the input of the CPS. The subradiance property manifests in a strongly nonmonotonic variation of these current resonances with the amplitude of the microwave signal applied to one of the two CPS dots. This behavior does not depend on details of the model like the exact form of the spin-orbit interaction term. Similarly, the presence of atomic disorder in the nanotube has to be assumed only for quantitative reasons. More generally, the entanglement detection scheme discussed in this work could be generalized to other types of quantum dots with spin-orbit coupling like, e.g., InAs nanowire based quantum dots, in principle. For simplicity, this article discusses the limit where the intradot charging energies are very strong, so that there cannot be two electrons at the same time on the same dot. For smaller charging energies, the efficiency of Cooper pair splitting should be decreased. Nevertheless, if the CPS produces entangled split Cooper pairs with a sufficient rate, the resulting subradiant current peaks should still be observable. Interestingly, the bonding or antibonding single particle states delocalized on the two dots of the CPS can also cause a subradiant current resonance, because they present another type of entanglement. However, in principle, this resonance can easily be discriminated from the subradiant resonances caused by split Cooper pairs, because of a different dependence on the CPS dc gate voltages.

ACKNOWLEDGMENTS

Author acknowledges useful discussions with T. Kontos, J. Viennot, and A. Levy Yeyati. This work has been financed by the EU-FP7 project SE2ND[271554].

[1] A. Aspect, P. Grangier, and G. Roger, Phys. Rev. Lett. **49**, 91 (1982); **49**, 1804 (1982).

[2] A. Rauschenbeutel, G. Nogues, S. Osnaghi, P. Bertet, M. Brune, J.-M. Raimond, and S. Haroche, Science **288**, 2024 (2000).

[3] C. A. Sackett, D. Kielpinski, B. E. King, C. Langer, V. Meyer, C. J. Myatt, M. Rowe, Q. A. Turchette, W. M. Itano, D. J. Wineland, and C. Monroe, Nature (London) **404**, 256 (2000).

[4] M. S Steffen, M. Ansmann, R. C. Bialczak, N. Katz, E. Lucero, R. McDermott, M. Neeley, E. M. Weig, A. N. Cleland, and J. M. Martinis, Science **313**, 1423 (2006); L. DiCarlo, J. M. Chow, J. M. Gambetta, Lev S. Bishop, B. R. Johnson, D. I. Schuster, J. Majer, A. Blais, L. Frunzio, S. M. Girvin, and R. J. Schoelkopf, Nature (London) **460**, 240 (2009); M. Neeley, R. C. Bialczak, M. Lenander, E. Lucero, M. Mariantoni, A. D. O'Connell, D. Sank, H. Wang, M. Weides, J. Wenner, Y. Yin, T. Yamamoto, A. N. Cleland, and J. M. Martinis, *ibid.* **467**, 570 (2010); L. DiCarlo, M. D. Reed, L. Sun, B. R. Johnson, J. M. Chow, J. M. Gambetta, L. Frunzio, S. M. Girvin, M. H. Devoret, and R. J. Schoelkopf, *ibid.* **467**, 574 (2010); A. Palacios-Laloy, F. Mallet, F. Nguyen, P. Bertet, D. Vion, D. Esteve, and A. Korotkov, Nat. Phys. **6**, 442 (2010).

[5] J. Q. You and F. Nori, Nature (London) **474**, 589 (2011).

[6] P. Recher, E. V. Sukhorukov, and D. Loss, Phys. Rev. B **63**, 165314 (2001).

[7] L. Hofstetter, S. Csonka, J. Nygard, and C. Schönenberger, Nature (London) **461**, 960 (2009).

[8] L. Hofstetter, S. Csonka, A. Baumgartner, G. Fülöp, S. d'Hollosy, J. Nygård, and C. Schönenberger, Phys. Rev. Lett. **107**, 136801 (2011).

[9] J. Schindele, A. Baumgartner, and C. Schönenberger, arXiv:1204.5777.

[10] L. G. Herrmann, F. Portier, P. Roche, A. L. Yeyati, T. Kontos, and C. Strunk, Phys. Rev. Lett. **104**, 026801 (2010).

[11] L. G. Herrmann, P. Burset, W. J. Herrera, F. Portier, P. Roche, C. Strunk, A. Levy Yeyati, and T. Kontos, arXiv:1205.1972.

[12] A. Das, Y. Ronen, M. Heiblum, D. Mahalu, A. V. Kretinin, and H. Shtrikman, arXiv:1205.2455.

[13] T. Martin, Phys. Lett. A **220**, 137 (1996).

[14] M. P. Anantram and S. Datta, Phys. Rev. B **53**, 16390 (1996).

[15] G. Burkard, D. Loss, and E. V. Sukhorukov, Phys. Rev. B **61**, 16303(R) (2000).

[16] G. B. Lesovik, T. Martin, and G. Blatter, Eur. Phys. J. B **24**, 287 (2001).

[17]J. Borlin, W. Belzig, and C. Bruder, Phys. Rev. Lett. **88**, 197001 (2002).
[18]P. Samuelsson and M. Büttiker, Phys. Rev. Lett. **89**, 046601 (2002).
[19]N. M. Chtchelkatchev, G. Blatter, G. B. Lesovik, and T. Martin, Phys. Rev. B **66**, 161320(R) (2002).
[20]O. Sauret, T. Martin, and D. Feinberg, Phys. Rev. B **72**, 024544 (2005).
[21]D. Chevallier, J. Rech, T. Jonckheere, and T. Martin, Phys. Rev. B **83**, 125421 (2011).
[22]J. Rech, D. Chevallier, T. Jonckheere, and T. Martin, Phys. Rev. B **85**, 035419 (2012).
[23]A. Cottet, T. Kontos, and A. L. Yeyati, Phys. Rev. Lett. **108**, 166803 (2012).
[24]M. R. Delbecq, V. Schmitt, F. D. Parmentier, N. Roch, J. J. Viennot, G. Fève, B. Huard, C. Mora, A. Cottet, and T. Kontos, Phys. Rev. Lett. **107**, 256804 (2011).
[25]T. Frey, P. J. Leek, M. Beck, A. Blais, T. Ihn, K. Ensslin, and A. Wallraff, Phys. Rev. Lett. **108**, 046807 (2012).
[26]Z.-L. Xiang, S. Ashhab, J. Q. You, and F. Nori, arXiv:1204.2137.
[27]T. S. Jespersen, K. Grove-Rasmussen, J. Paaske, K. Muraki, T. Fujisawa, J. Nygård, and K. Flensberg, Nat. Phys. **7**, 348 (2011).
[28]W. Liang, M. Bockrath, and H. Park, Phys. Rev. Lett. **88**, 126801 (2002).
[29]F. Kuemmeth, S. Ilani, D. C. Ralph, and P. L. McEuen, Nature (London) **452**, 448 (2008).
[30]A. Pályi and G. Burkard, Phys. Rev. Lett. **106**, 086801 (2011).
[31]J. Eldridge, M. G. Pala, M. Governale, and J. König, Phys. Rev. B **82**, 184507 (2010).
[32]See Supplemental Material of Ref. 23 at http://link.aps.org/supplemental/10.1103/PhysRevLett.108.166803.
[33]W. Izumida, K. Sato, and R. J. Saito, Phys. Soc. Jpn. **78**, 074707 (2009).
[34]J. Klinovaja, M. J. Schmidt, B. Braunecker, and D. Loss, Phys. Rev. B **84**, 085452 (2011).
[35]D. Huertas-Hernando, F. Guinea, and A. Brataas, Phys. Rev. B **74**, 155426 (2006).
[36]T. Ando, J. Phys. Soc. Jpn. **69**, 1757 (2000).
[37]A. DeMartino, R. Egger, K. Hallberg, and C. A. Balseiro, Phys. Rev. Lett. **88**, 206402 (2002).
[38]D. V. Bulaev, B. Trauzettel, and D. Loss, Phys. Rev. B **77**, 235301 (2008).
[39]J.-S. Jeong and H.-W. Lee, Phys. Rev. B **80**, 075409 (2009).
[40]P. Recher, Y. V. Nazarov, and L. P. Kouwenhoven, Phys. Rev. Lett. **104**, 156802 (2010).
[41]F. Godschalk, F. Hassler, and Y. V. Nazarov, Phys. Rev. Lett. **107**, 073901 (2011).
[42]O. Sauret, D. Feinberg, and T. Martin, Phys. Rev. B **70**, 245313 (2004).
[43]C. Meyer, J. M. Elzerman, and L. P. Kouwenhoven, Nano Lett. **7**, 295 (2007).
[44]Note that, in principle, the term $H^g_{\rm RF}$ can induce transitions $|a_{i\sigma}\rangle \leftrightarrow |b_{i\sigma}\rangle$ at the frequency $2t_{\rm ee}/\hbar$. However, the states $|a_{i\sigma}\rangle$ and $|b_{i\sigma}\rangle$ have similar weights in $|K\sigma,0\rangle$, $|0,K\sigma\rangle$, $|K'\sigma,0\rangle$, and $|0,K'\sigma\rangle$. Therefore these transitions should not be visible in the CPS input current.
[45]M. Trif, V. N. Golovach, and D. Loss, Phys. Rev. B **77**, 045434 (2008).